Available online at www.sciencedirect.com
ScienceDirect
Journal of Power Sources 165 (2007) 774–785
JOURNAL OF POWER SOURCES
www.elsevier.com/locate/jpowsour

Monte-Carlo simulation and performance optimization for the cathode microstructure in a solid oxide fuel cell

Yan Ji, Kun Yuan, J.N. Chung *

Department of Mechanical and Aerospace Engineering, University of Florida, Florida 32611-6300, USA

Received 13 November 2006; received in revised form 15 December 2006; accepted 20 December 2006
Available online 12 January 2007

Abstract

A 3D micro-scale model is developed to simulate the transport and electrochemical reaction in a composite cathode. This model takes into account the details of the specific cathode microstructure such as random pore structure, active TPB (three phase boundary) site distribution, particle size and composition and their interrelationship to the charge transfer and mass transport processes. Especially, the pore structure and mass diffusion were incorporated into this model. Influence of the microsturcture parameters on the performance was investigated by numerical simulations.

Simulation shows that the cathode porosity should be in the range of 0.25–0.45 for the optimized performance. A larger thickness is in favor of increasing the effective reaction sites and reducing total specific resistance. However, the thickness needs to be confined below a certain thickness in order to prevent lower utilization and excessive concentration loss. The fine particles contribute to increase the TPB length and thus decrease the activation overpotential. On the other hand, the extremely small particles might lead to an excessive diffusion resistance. The model was validated based on the continuum model and experimental data to determine its accuracy in predicting the cathode performance. The results generally agree with the experimental data from the literature. However, as compared with the continuum model, the predicted total resistance is slightly higher for a thin electrode.

Keywords: Solid oxide fuel cell; Composite electrode; Optimization; Modeling

1. Introduction

Solid oxide fuel cells can provide clean and highly efficient energy utilization in wide applications from small stationary power units to larger scale capacities. Many investigations on the loss mechanisms by impedance spectroscopy as well as theoretical analysis have revealed that the cathode governs the main part of the losses and thus the improvement in electrochemical behavior strongly depends on selected material and microstructure of the cathode, etc. In the case of pure electronic-conducting electrode materials like metals or some perovskite type oxides (LSM), electrochemical reactions are almost confined to the triple phase boundaries (TPB, gas/electrolyte/electrode) [1,2]. The transport of oxide ions within the electrode materials is advantageous concerning the number of possible reaction pathways. Therefore, high performance electrodes should be composed of either a composite consisting of an electronic and an ionic conducting phase or a mixed conducting metal oxide to expand the active reaction area into the electrode volume. The performance of a composite electrode is determined by the following factors: (1) conductivities of pure ionic and electronic conductors, (2) specific surface area available for electrochemical reaction (or the size of TPB), (3) microstructure of electrode, i.e., the compositional volume ratio, porosity and particle size distribution, and (4) path of gas diffusion. For example, Kim et al. [3] indicated that polarization resistance of the LSM–YSZ composite electrodes is closely related to the connectivity of LSM–YSZ particles and depends on their size ratio. The composite electrode showed low electrochemical activity without YSZ connectivity. However, the polarization resistance decreased abruptly when the YSZ connectivity is present. Thus, optimization of conductivity and polarization resistance of composite electrodes for a SOFC in terms of the microstructure will undoubtedly gain substantial understanding.

* Corresponding author. Tel.: +1 352 392 9607; fax: +1 352 392 1071.
E-mail address: jnchung@ufl.edu (J.N. Chung).

0378-7753/$ – see front matter © 2007 Elsevier B.V. All rights reserved.
doi:10.1016/j.jpowsour.2006.12.058

Nomenclature

B^e	diffusion matrix
$\vec{C}$	mass concentration vector (kg m^{-3})
D_c	diameter (m)
D_{ij}^b	binary mass diffusivity (m^2 s^{-1})
D_{ii}^K	effective Knudsen diffusion coefficient for component i (m^2 s^{-1})
F_1	Forchheimer coefficient
i_{tr}	exchange current density of cathode (A m^{-1} or A m^{-2})
I	current flow (A)
$\vec{J}$	diffusion mass flux vector
L_x, L_y, L_z	dimensions of electrode (m)
M_i	molar weight of component i (kg mol^{-1})
N_x, N_y, N_z	size of lattice in x, y and z directions
p	pressure (Pa)
$p_{O_2}^r$	partial pressure of oxygen at reaction site (atm)
$\bar{r}_p$	aveage pore radius (m)
$\dot{R}$	rate of consumed mass (kg m^{-3} s^{-1})
R_g	universal gas constant, 8.3143 J mol^{-1} K^{-1}
R_{tot}	total resistance (Ω)
T	temperature (K)
X_i	molar fraction of component i

Greek letters

β	transfer coefficient
δ	neck of diameter (m)
ε	porosity
ϕ	potential (V)
γ	contact angle (°)
η_{act}	activation overpotential (V)
η_{con}	concentration overpotential (V)
κ_{io}, κ_{el}	ionic conductivity, electronic conductivity (Ω^{-1} m^{-1})
μ	viscosity (m^2 s^{-1})
σ	electrical or ionic conductance (Ω^{-1})
ω_{ij}	characteristic length
Ω_D	collision integral
ξ	coordinate of the pore
$\Delta\xi_{i-I}$	distance for any two neighbor particles (m)
ℓ	neck circumference (m)

Subscripts

el	electronic
io	ionic

However, the microstructure of an electrode is not regular and thus all mass and energy transport within electrodes take place in a disordered, unorganized medium. This random characteristic makes modeling electrode become extremely difficult, because the accuracy of a model is dependent on how to describe this random geometry. One of the representative publications is Costamagna et al.'s continuum model [4] based on the percolation theory and coordination number theory [5–10]. This statistical method gives a good starting point for composite electrode simulation due to simplicity and explicity; however, some inherent assumptions and oversimplifications limit the application range of this type of continuum-model: (1) the mass resistance in a porous medium is completely neglected from the assumptions of faster diffusion and smaller particle size. However when the thicknesses of electrode or current density are greater, the overpotential due to mass resistance is not negligible. (2) Since only sample-spanning electrolyte and electrode cluster are accounted for in this model, the theory is not valid outside the composition regime in which isolated clusters are present and has lower ratio of thickness to particle radius. (3) The mechanism of electrochemical reaction was not investigated. In order to further apply the continuum-model to actual SOFC electrodes, some modifications are proposed by Chan et al. [11]. The primary improvement is the electrochemical reaction in which the exchange current density is not constant as in previous work. Jeon et al. [12] extended the original model to an actual multilayer electrode.

Obviously, the most natural modeling methodology is directly based on the actual microstructure of such composite electrodes. In principle, any disordered system can be mapped onto a random network of bonds connected to each other at sites or nodes of the network. The network models incorporate pore-scale descriptions of the medium and the physics of pore-scale events [13–20]. This method represents the type of approach that best predicts the most important experimental features of composite electrodes. However, their models suffered from some common weaknesses. These models overemphasize the effect of selected parameters on the performance and do not comprehensively evaluate the overall performance. Further, the influence of pore distribution, thermal factor and current distribution are rarely considered.

Therefore, reliable models capable of handling realistic microstructural features and mass/heat transport are essential for establishing a quantitative relationship between the microstructure and the electrical properties in composite electrodes. Accordingly, a micro-scale model considering more detailed mass and energy transport processes will be developed in the present paper. A novel 3D random walk model will be applied to optimize the performance in a porous composite cathode resulting in a complete description of the electrode structure as well as the processes occurring therein. The pore distribution, composition, mass diffusion and current density distribution, etc. will be completely integrated into the micro-model.

2. Physical description and assumptions for micro-model

The networks of porous cathode are complex, and in practice it is necessary to adopt simplified models which reproduce the essential features, but ignore many of the details, of a real network. In the present model, an idealized 3D microstructure is constructed as shown in Fig. 1 (only 2D view is given). The microstructure takes the form of a face-centered cubic lattice (FCC). This kind of structure represents a dense packing of particles of the same size (i.e., electrolyte, electrode and pores). A

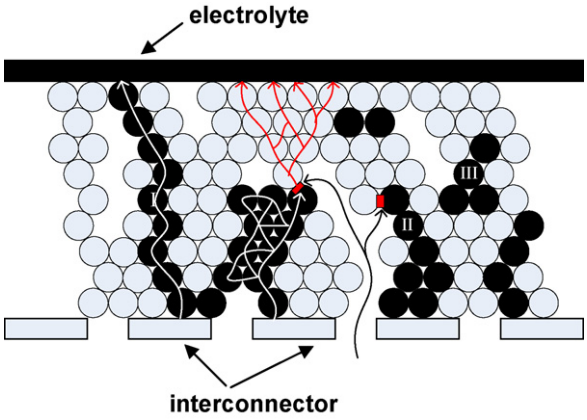

Fig. 1. 2D view of random network model. Red rectangle denotes the active TPB; black circle, electronic conductor; blue circle, ionic conductor; white empty, pore (the circles have been removed for clarify). Three paths along the three phases for gas (black), O^- (red) and e^- (white) are represented by curves. (For interpretation of the references to color in this figure legend, the reader is referred to the web version of the article.)

practical cathode has a random topology, i.e., its local coordination number, which is the number of bonds connected to a site, is a chaotic and almost random variable. Sunde [18,19], Zalc et al. [15], Constantinides et al. [21] and Ciobanu et al. [22] employed the arbitrary resistor network with non-uniform grain size and shape to represent the porous structures. However, some studies [23,24] have demonstrated that as long as the average coordination number of the topologically disordered network is equal to the coordination number of a topologically regular network, transport and main properties are identical for the two network systems. Therefore, a 3D regular lattice is used here. The spatial distributions of grain particles and pores are still random. In Fig. 1, blue, black, and white sites represent the electrolyte, electrode and pore particles, respectively. The electrons from inter-connector through electrolyte clusters and the oxygen through contiguous pore passage are supplied to the active TPB (explained later), where the oxygen ions are generated by electrochemical reactions. Then the oxygen ions are transferred to the electrolyte membrane by electrode clusters. In developing this model, several assumptions and definitions are made and summarized as follows:

(1) Not all of pores are "open" for reaction. Some of pores may be inaccessible to one or more of the species so that the effective TPB length and effective diffusivity are reduced. When the porosity is small, the pore forms small and isolated clusters. As the porosity is increased enough, there would be some clusters spanning the network from one end to the other. This kind of pore clusters is termed as "transport pore" cluster, since it allows the gas to transport across the entire medium. A pore belonging to a "transport pore" cluster is called a "transport pore". The second kind of pores, which is called "dead-end pore", is interconnected only from one side (current collector). Although these pores can often be penetrated, their contribution to transport is negligible to transport. The third kind of pores is "isolated pore", which is totally isolated from its neighbors of "transport pore" and cannot contribute to transport of mass cross the porous medium. Here, this common realistic situation is considered and pores are randomly distributed and identified as "transport", "dead-end" or "isolated" pores.

(2) Three types of clusters in a solid phase, i.e., "percolating cluster" (I), "singly connected cluster" (II) and "isolated cluster" (III) are identified. The first kind of clusters, i.e., a percolating cluster, is that the same type of particles (ionic or electronic particles) touches one another to extend through the entire electrode. Under such a condition, a good conductivity is reached. The second is that a cluster is only connected to its corresponding bulk phase type (i.e., interconnector or electrolyte). The last kind of clusters, "isolated cluster", is completely isolated from its corresponding bulk phase. The existence of this kind of clusters increases the polarization resistance in the electrode. The distribution of these clusters in electrodes is strongly influenced by the particle ratio, the volume ratio and sintering process, etc.

(3) Gas is considered to be an ideal two-component mixture of O_2 and a dilute gas (N_2). Within the pores, there are three distinct diffusion mechanisms for mass transfer [25]: molecular diffusion, Knudsen diffusion and surface diffusion of adsorbed molecular species along the pore wall surface. The molecular and Knudsen diffusion are dominant mechanisms at the cathode and will be taken into account in this model.

(4) Only the dc part of the effective electronic conductivity is considered. The ac part of the conductivity due to double layer effect (i.e., capacitance effect) is neglected.

(5) The cathodic reaction site is limited to the vicinity of an "active bond". This concept is firstly introduced by Alder et al. [26]. The bond between two neighboring sites, one of which is an electrolyte and the other an electrode site, is active if both of the sites belong to a "percolating cluster" or a "singly connected cluster" and also the bond has a neighboring empty site (pore), which belongs to the "transport pore" cluster or "dead-end pore" cluster.

(6) Isothermal and steady-state operation.

3. Derivation of numerical model

According to the conservation principle, the current flux entering a control volume should be equal to those leaving this volume plus the stored current within it. Therefore, the governing equations for charge transport in the solid phase (two phases) and gas species transport in the void space, respectively, are:

$$\nabla \cdot (\sigma_{\text{eff}} \nabla \phi) = 0 \tag{1}$$

$$\nabla \cdot \vec{J}_{\text{tot}} + \dot{R} = 0 \tag{2}$$

Here ϕ and $\vec{J}_{\text{tot}}$ are the electrical potential within solid particles and total mass flux vector, respectively. $\dot{R}$ is the rate of consumed mass due to an electrochemical reaction. σ_{eff} is the effective conductance. The values of conductance in the solid phase are finite and zero in the gas phase, respectively. Actually, Eq. (1) is applied to both of the two solid phases and Eq. (2) is valid for pore space. The two equations are coupled by electrochemical reaction on the active three phase boundary. Hence, the

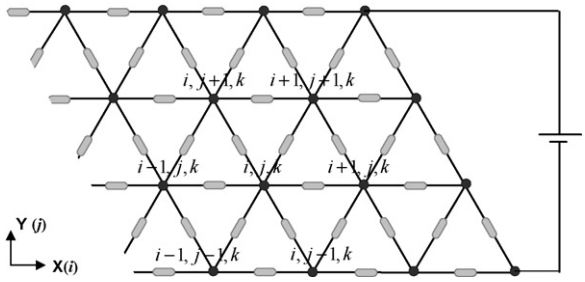

Fig. 2. Schematic of electrical network.

idealized random microstructure can be considered to split into two sub-networks: an electrical network for the solid phase and a pore network on the void space. The species concentrations and chemical reaction rate (Eq. (2)) will be calculated within the pore network, whereas the charge transfer, resistances and overpotentials (Eq. (1)) will be analyzed within the electrical networks.

3.1. Electrical network

Fig. 2 illustrates a two-dimensional electrical network. Nodes (i, j, k) represent solid particle sites. Between each pair of solid particles, the current is conducted through a resistance with the "effective conductance σ_{eff}". There are three kinds of conductances: the conductance between the electrolyte particles $\sigma_{\text{io–io}}$, the conductance between the electrode particles $\sigma_{\text{el–el}}$ and the conductance between two different particles $\sigma_{\text{io–el}}$. Here, subscript "io" refers to the electrolyte and "el" to the electrode particles. These conductances depend on the neck formed by the contact between two particles. A neck of diameter 2δ is formed between two contacting spheres with the same radius r and thus the neck circumference, ℓ, is equal to $2\pi\delta$. The conductance between the same types of particles can be approximated as

$$\sigma_{\text{io–io}} = \frac{\kappa_{\text{io}}\ell_{\text{io–io}}}{4}, \qquad \sigma_{\text{el–el}} = \frac{\kappa_{\text{el}}\ell_{\text{el–el}}}{4} \tag{3}$$

where κ_{io} and κ_{el} are the ionic conductivity and electronic conductivity, respectively, which are dependent on the temperature. The conductance $\sigma_{\text{io–el}}$ between different types of particles is given below based on linear electrochemical kinetics [18,19]:

$$\sigma_{\text{io–el}} = \left[\frac{1}{2\sigma_{\text{el–el}}} + \frac{1}{2\sigma_{\text{io–io}}} + \frac{1}{\sigma_{\text{p}}}\right]^{-1} \tag{4}$$

where σ_{p} is the polarization conductance. For an inactive TPB, σ_{p} is set as infinity. While for an active TPB, σ_{p} depends on the geometry of a TPB and the activity of a cathodic reaction. In previous works [12,18], σ_{p} was assumed to be a constant and proportional to the polarization conductivity κ_{p} and three phase boundary length ℓ_{TPB}. However, Sunde [18] has implied that his model has significant error due to neglecting the effect of gas diffusion on the electrochemical reaction and κ_{p} determined by a simplified geometry, not the electrolyte–electrode contacts in the composite. Thereafter, a new approach is used in this paper to evaluate this value considering the effect of gas diffusion, temperature, chemical reaction and TPB geometry. η_{act} is the activation overpotential and expressed by

$$\eta_{\text{act}} = \phi_{\text{el}} - \phi_{\text{io}} - \Delta\phi_{\text{conc}} \tag{5}$$

So the polarization conductance corrected for ohmic drop can be expressed by

$$\sigma_{\text{p}} = \left(\frac{\eta_{\text{act}}}{i_{\text{tr}}\ell_{\text{TPB}}}\right)^{-1} = \left(\frac{\phi_{\text{el}} - \phi_{\text{io}} - \Delta\phi_{\text{conc}}}{i_{\text{tr}}\ell_{\text{TPB}}}\right)^{-1} \tag{6}$$

here ℓ_{TPB} is still equal to $2\pi\delta$ and also can be given by

$$\ell_{\text{TPB}} = 2\pi\delta = 2\pi r \sin\frac{\gamma}{2} \tag{7}$$

where r is the radius of the particle and γ is the contact angle between ionic and electronic conductors. Chan et al. [11] found that this angle can be reasonably estimated as 60°. The concentration overpotential is therefore calculated as [27]

$$\Delta\phi_{\text{conc}} = \frac{R_{\text{g}}T}{4F}\ln\left(\frac{p_{\text{O}_2}^{\text{int}}}{p_{\text{O}_2}^{\text{r}}}\right) \tag{8}$$

where $p_{\text{O}_2}^{\text{int}}$ and $p_{\text{O}_2}^{\text{r}}$ are the partial pressures of oxygen at cathode/channel interface and reaction site (TPB), respectively.

In Eq. (6), there is still one parameter, the exchange transfer current, i_{tr}, left to be determined. As a matter of fact, oxygen reduction reaction has been recognized to involve a series of consecutive elemental steps including, i.e., dissociation, charge transfer, surface diffusion of oxygen intermediate species, and incorporation of oxygen ions into the YSZ electrolyte. The current density depends on the partial oxygen pressure, rate constants in elementary reaction steps, detailed experimental condition and microstructure of electrodes, etc. It is difficult to evaluate this value theoretically; instead, fitting from experimental data is generally used [11]:

$$i_{\text{tr}} = f(T, p_{\text{O}_2}, \eta_{\text{act}}) = 7874 \times p_{\text{O}_2}^{1/4} \times \exp\left(-\frac{2.05\times10^4}{T}\right) \times\{\exp(f\eta_{\text{act}}) - \exp(-f\eta_{\text{act}})\} \tag{9}$$

here $p_{\text{O}_2}$is the partial oxygen pressure, and T is the absolute temperature. $f = F/R_{\text{g}}T$, where R_{g} is the gas constant and F is the Faraday's constant. Finally, the current conservation equation (Eq. (1)) can be replaced by the following discretized form:

$$\sum_j I_{i\to j} = \sum_j \sigma_{ij}(\phi_i - \phi_j) = 0 \tag{10}$$

where ϕ_i and ϕ_j are the potentials for particle i and its neighbors j, respectively. $I_{i\to j}$ denotes the current flowing from site i to its neighboring site j. σ_{ij} is the conductance between sites i and j. By iteratively solving Eqs. (3)–(9), the distribution of potential in the composite cathode can be obtained. Once the potential distribution is determined, the total resistance for the cathode is estimated as

$$R_{\text{tot}} = \frac{\phi_{\text{top}} - \phi_{\text{bot}}}{I_{\text{total}}} \tag{11}$$

It should be noted that the total resistance includes all three overpotentials, i.e., ohmic loss, activation loss and concentration loss. If the polarization conductivity is set to be infinite ($\sigma_p = \infty$), the total ohmic resistance R_{ohm} will be easily evaluated. Then, the total polarization resistance R_p is obtained by subtracting R_{ohm} from R_{tot}, i.e., $R_p = R_{tot} - R_{ohm}$.

3.2. Diffusion and reaction rate

There are three diffusion mechanisms that exist within the voids. The total flux of any species is obtained by combining the separate contributions. Because the bulk and Knudsen diffusion are dominant mechanisms in the composite cathode which has larger particle sizes (0.1–5 μm), therefore the surface diffusion is neglected in this model. The total mass transfer in a single pore is a sum of diffusive and viscous flux ($kg\,m^{-2}\,s^{-1}$):

$$\vec{J}_{tot} = \vec{J}_{diff} + \vec{J}_{vis} \tag{12}$$

The first term on the right hand side ($\vec{J}_{diff}$) is the mass flux due to bulk and Knudsen diffusion, which can be expressed by a N-dimensional matrix notation:

$$\vec{J}_{diff} = -[B^e(r_p, \vec{C})]^{-1} \frac{d\vec{C}}{d\xi} \tag{13}$$

where $\vec{C}$ and ξ are the mass concentration vector and coordinate of the pore, respectively. The $N-1$ dimensional square matrix $[B^e]$ has the elements:

$$B^e_{ij(i\neq j)} = -\frac{X_i}{D^b_{ij}}, \qquad B^e_{ii} = -\frac{1}{D^K_{ii}} + \sum_{k=1,k\neq i}^{N-1} \frac{X_k}{D^b_{ik}} \tag{14}$$

here X_i represents the mole fraction of component i, D^b_{ij} the binary diffusivity of components i and j, and D^K_{ii} is the effective Knudsen diffusivity of component i. N is the total number of components. Both of the two diffusivities can be calculated as

$$D^k_{ii} = \frac{2}{3}\sqrt{\frac{8R_gT}{\pi M_i}}\bar{r}_p \tag{15}$$

$$D^b_{ij} = 1.86\times10^{-7}\frac{[T^3(M_i+M_j)/M_iM_j]^{1/2}}{p\omega^2_{ij}\Omega_D} \tag{16}$$

where ω_{ij} is the characteristic length, and Ω_D is the collision integral. The viscous flux in Eq. (11) is given by the following expression:

$$\vec{J}_{vis} = -\vec{C}\cdot\frac{\bar{r}^2_p}{8\mu}RT\cdot\frac{dC_{tot}}{d\xi} \tag{17}$$

here μ is the viscosity and T is the temperature. C_{tot} is the total molar concentration and given by

$$C_{tot} = \sum_{i=1}^{N}\frac{C_i}{M_i} \tag{18}$$

The volumetric source term $\dot{R}$ ($kg\,m^{-3}\,s^{-1}$) due to electrochemical reaction is related to the transfer current density i_{tr} (Eq. (5)), TPB length and pore size, which can be expressed by

$$\dot{R} = \frac{i_{tr}\ell_{TPB}}{(4/3)\pi\bar{r}^3_p\cdot 4F} \tag{19}$$

It is apparent that only the gas phase site having active TPB has the source term $\dot{R}$. The pore structure can be treated as a three-dimensional pore network, and the single pores are connected at the nodes of the network. The flux of each species that enters a node must be equal to the flux leaving the node plus the accumulative mass. Therefore, at the inner nodes of the network, an equation similar to the Kirchhoff's law holds:

$$\sum_{i\in M}\nabla\cdot\rightarrow J_{i\rightarrow I} = \dot{R}_I \tag{20}$$

where M denotes all the pores that are connected to node I, and $\rightarrow J_{i\rightarrow I}$ are fluxes leaving or entering node I. Actually, Eq. (20) is the discritized form of Eq. (2). For a two binary component system (O_2 and N_2), Eq. (20) can be rewritten in the following expression by combining Eqs. (13) and (17):

$$\sum_{i\in M}\left\{C_{O_2,I}\cdot\frac{\bar{r}^2_p}{8\mu}RT\cdot\frac{C_{tot,i}-C_{tot,I}}{\Delta\xi_{i-I}}\right\}\times\frac{D^2_c}{(16/3)\bar{r}^3_p} + \sum_{i\in M}\left[\frac{1}{D^K_{O_2}}+\frac{1-\alpha X_{O_2,I}}{D_{O_2,N_2}}\right]\cdot\frac{C_{O_2,i}-C_{O_2,I}}{\Delta\xi_{i-I}}\times\frac{D^2_c}{(16/3)\bar{r}^3_p} = \dot{R}_I \tag{21}$$

where

$$\alpha = 1-\left(\frac{M_{O_2}}{M_{N_2}}\right)^{1/2} \tag{22}$$

$\Delta\xi_{i-I}$ is the distance between any site I and any neighboring pore i. $X_{O_2,I}$ is the molar fraction of oxygen at site I. In this model, each pair of any two neighboring sites are assumed to be connected by a cylindrical channel with length $\Delta\xi_{i-I}$ and diameter D_c. Finally, Eqs. (10) and (20) have to be solved simultaneously by a finite difference scheme for the entire network.

4. Reconstruction of microstructure and boundary conditions

Fig. 3 shows a typical constructed microstructure for the $24\times24\times18$ cubic FCC lattice. The size of the lattice is represented by N_x, N_y and N_z layers in the x, y, and z directions, respectively. The z-direction is taken as the primary direction of current flow, and the dimension in this direction, is by definition equal to the thickness of electrode, L_z. The radius of a particle is in the range from 0.1 to 5 μm. Once the microstructure is constructed, the connectivity and the different clusters need to be identified. For this purpose,

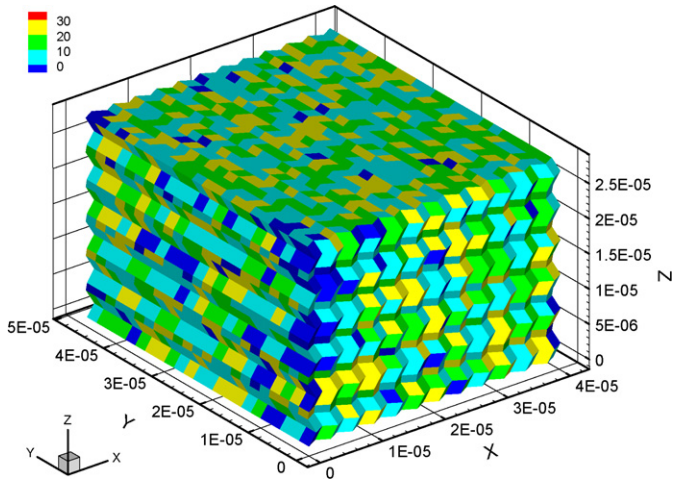

Fig. 3. Reconstruct of 3D random microstructure. Model parameters: $\varepsilon = 0.4$, ϕ_{el}:ϕ_{io} = 1:1, 24 × 24 × 18. Blue (0), isolated particle; cyan (10), transport pore; green (20), transport electronic particle; yellow (30), transport ionic particle. (For interpretation of the references to color in this figure legend, the reader is referred to the web version of the article.)

the Hoshen–Kopelman algorithm [16,28] is used to identify the "percolating cluster", "isolated cluster", "dead-end cluster" and "active TPB". All of the quantitative results will be obtained as an average over six different random microstructures with different seed numbers. Fig. 4(a) gives the local percentage variation for three different sites. These data suggest that the pore, electronic and ionic sites are randomly distributed across the thickness and the algorithm used to describe the microstructure is unbiased. All of the electrochemical variables in the z-direction are of interest, so the edge effect of x- and y-dimension on the electrochemical behavior should be minimized.

Fig. 4(b) shows the dependence of the effective porosity on the x and y dimensions. It shows that when the total number of cells in the x and y directions is increased from 24 to 36, the transport pore volume fraction varies only slightly. Therefore, the number of lattices is chosen at 24 that is considered to be sufficient in the x and y directions, so it is employed for the following calculations. Also, it is noted that when the natural porosity is larger than 0.3, the effective porosity is almost identical to the natural porosity. However, when the natural porosity is larger than 0.5, the volume fraction of "transport" solid particles (electronic and ionic) dramatically decreases since the "isolated" and "dead-end" solid clusters dominate the whole electrodes. Therefore, it is concluded that 0.3 is the lower bound of the porosity. In practical applications, the porosity is always in the range of 0.35–0.45.

The boundary before the first z layer represents the equipotential surface of the current collector (metal), which means that all bonds connected with it are linked to the metal and gas transport channels and the potential is set as ϕ_0. The boundary after the last z layer contacts the solid bulk electrolyte membrane, which stands for another equipotenal surface and is set to be at zero voltage. In the x and y directions, symmetric boundary conditions are employed. The boundary conditions are summarized

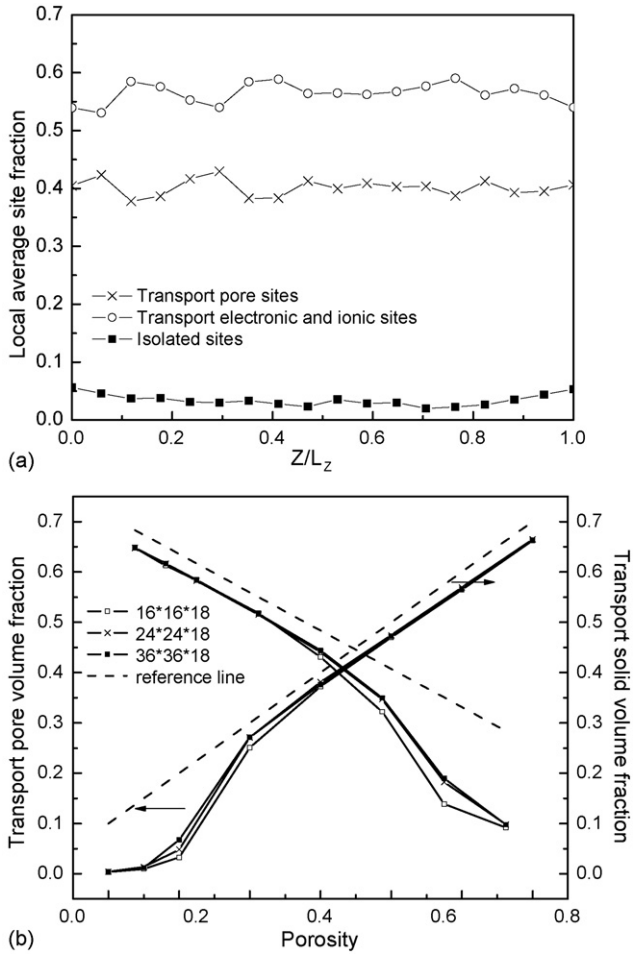

Fig. 4. Statistics of random microstructure (model parameters: $\varepsilon = 0.4$, ϕ_{el}:ϕ_{io} = 1:1): (a) local variation in three kind of sites along the thickness; (b) effects of cross-sectional mesh resolution on the transport pore volume fraction and transport solid volume fraction.

as below:

$$\text{At} \quad x = 0, \quad y = 0, \quad x = L_x,$$
$$y = L_y : \frac{\partial C_{O_2}}{\partial n} = 0, \quad \frac{\partial \phi}{\partial n} = 0 \tag{23a}$$

At the electrode/metal interface

$$z = 0 : C_{O_2} = C_{O_2,0}, \quad \phi_{el} = \phi_0, \quad I = I_{tot} \tag{23b}$$

At the electrolyte/cathode interface

$$z = L_z : \frac{\partial C_{O_2}}{\partial n} = 0, \quad \phi_{io} = 0 \tag{23c}$$

Note that in Eq. (23b), only the potentials for electrode particles are set as finite values, and the potentials for electrolyte particles should be considered as "inner nodes" and obtained by solving the governing equations. Similar cases hold for boundary condition (23c). The input parameters, including the transport and kinetic parameters are extracted from literatures [4,11,27] and listed in Table 1. The conductivities for LSM and YSZ are considered to be dependent on the temperature. Air (79% N_2 and 21% O_2) is delivered to cathode.

Table 1
Model input parameters for the baseline case

Parameters	Value	Parameters	Value
Air inlet temperature (K)	1100	Contact angle, γ	60°
LSM conductivity (S m^{-1})	$(8.855 \times 10^7/T) \times \exp(-1092.5/T)$	YSZ conductivity (S m^{-1})	$3.34 \times 10^5 \times \exp(-10300/T)$
External voltage difference (V)	0.2	Bulk oxygen concentration (kg m^{-3})	0.0825
$L_x \times L_y \times L_z$	$24 \times 24 \times 18$	Particle diameter (μm)	2×10^{-6}
Porosity	0.4		

5. Numerical results and discussions

5.1. Contours of potential and oxygen concentration

To study the potential distribution, the mass diffusion and the significance of overpotentials around the overall cathode region, we first select a microstructure with the seed number "2" and "3" as the baseline case. Although results obtained from this random microstructure is different from that based on an average of several microstructures with different seed numbers, the errors are so small that will not significantly change the values of potential and oxygen concentration. In this case, the external voltage difference is set as 0.2 V, the porosity is 0.4 and the composition ratio of electrode phase is 0.5. The average current density is calculated as 0.806 A cm^{-2}. The 3D contours of potential are plotted in Fig. 5. It turns out that the potential in the ionic phase gradually decreases from about 0.11 V to zero across the electrode thickness (z-direction). For electronic phase (Fig. 5(b)), however, the variation in potential is almost negligible. These distributions attribute to the higher conductivity for LSM and very lower conductivity for YSZ. Such larger potential difference between LSM and YSZ is just caused by the electrochemical reaction in the vicinity of TPB. Distributions of corresponding average cross-sectional exchange density and polarization conductance through the cathode, normalized to the current and the polarization conductance at the first layer, are displayed in Fig. 6. In the present study, the exchange current is modeled as a function of activation overpotential, and other operation parameters, which is different from the assumption of constant value in Sun's study [18,19]. The exchange current density monastically increases and reaches the peak value at the bottom of electrode. This tendency indicates that the strongest electrochemical reaction takes place on the region near the bottom end of the cathode, where the larger potential difference and maximal number of active TPB exist. For pure phase cathode, the electrochemical reaction is only confined to a very narrow zone, i.e., the electrolyte/cathode interface; while for composite cathode, the ionic phase extends to the bulk LSM phase and hence increases the reaction sites. Also, we found that the higher active TPB number, the larger the polarization conductance is.

Fig. 7 compares the oxygen concentration under lower and higher potential differences. Under the lower potential difference, the oxygen concentration is fairly uniform, decreasing from 0.08259 kg m^{-3} to roughly 0.075 kg m^{-3} across the electrode thickness. While for the case of a higher potential difference, i.e., 0.4 V, the oxygen gradually decreases to a lower level of oxygen concentration due to a larger oxygen consumption rate. The uniform oxygen distribution on a x–y plane validates that the percolating cluster dominates the whole region and makes the oxygen well supplied to the active TPB.

5.2. Activation and concentration overpotentials

Fig. 8(a) illustrates the profiles of average ohmic and activation overpotentials with respect to different external voltages. An increase of voltage difference (i.e., average current density), the sum of ohmic and activation loss also increases. Although

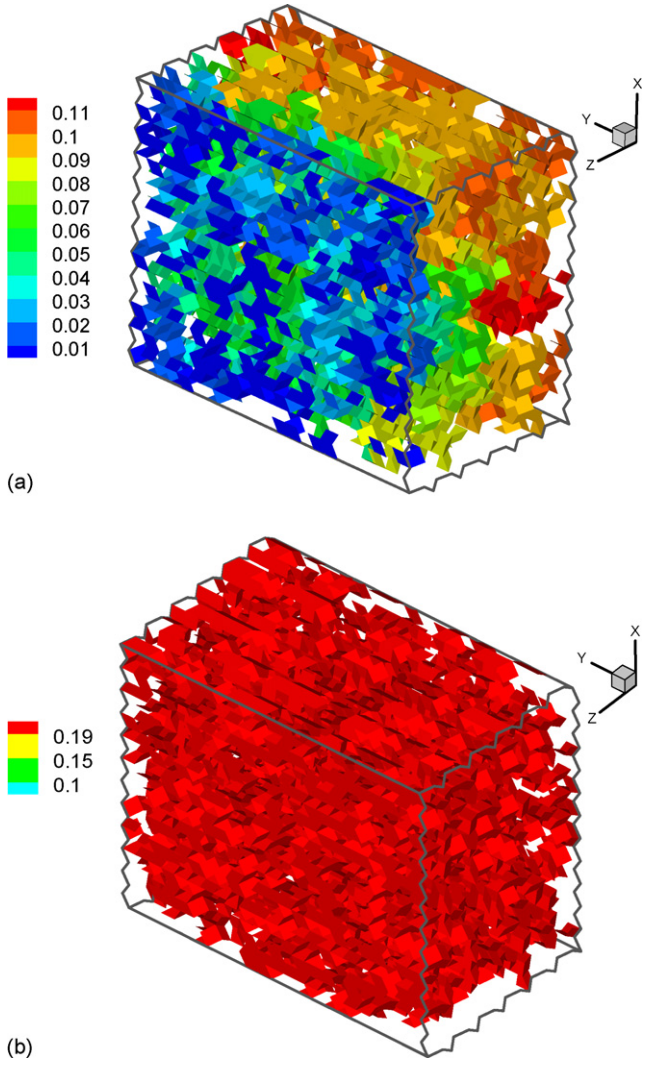

Fig. 5. 3D contours of potential (unit: V): (a) for electronic particles; (b) for ionic particles.

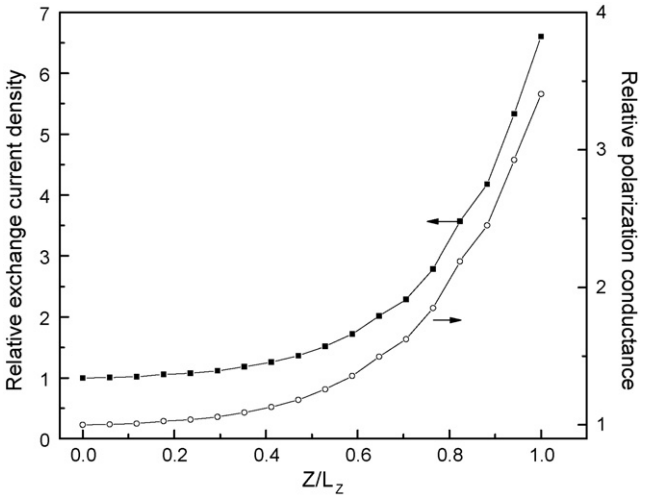

Fig. 6. Profiles of local relative exchange current density and relative polarization conductance.

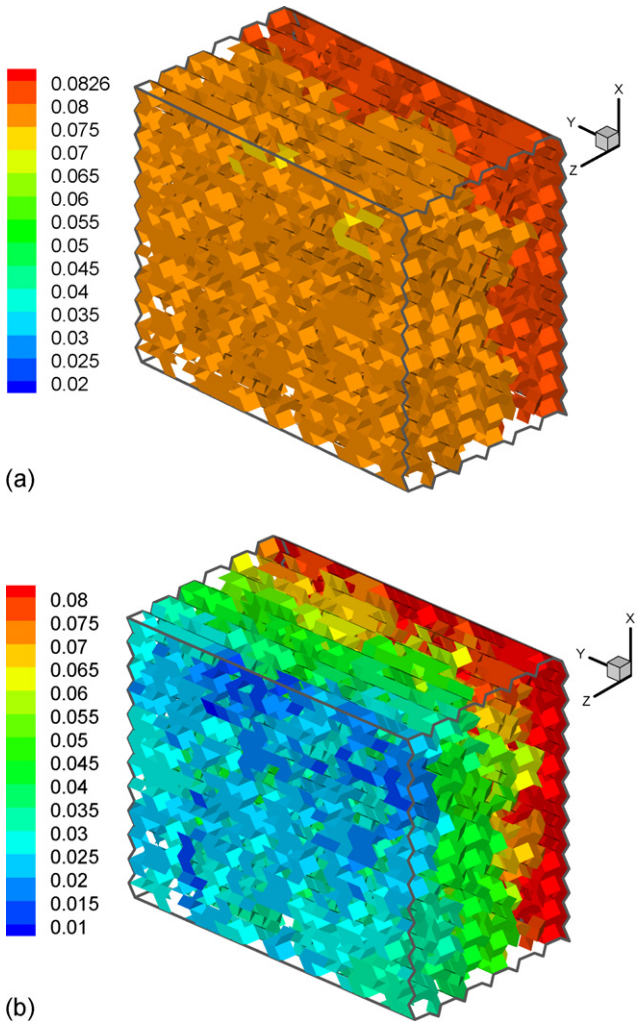

Fig. 7. 3D contours of oxygen concentration: (a) lower potential difference; (b) higher potential difference.

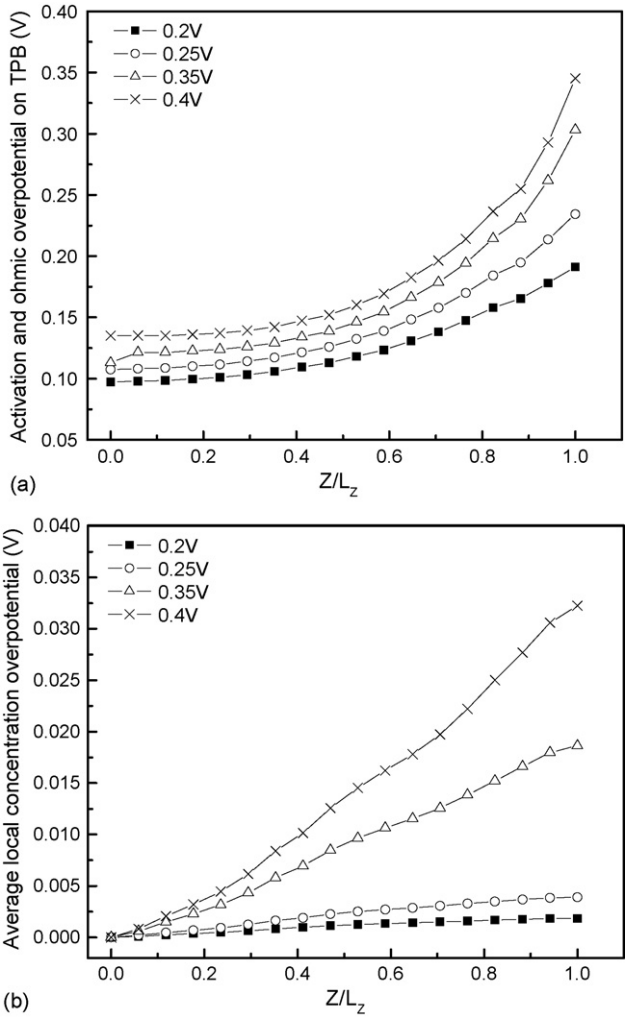

Fig. 8. Profiles of overpotential distributions: (a) ohmic and activation loss; (b) concentration loss.

both of the numbers of active TPB on the gas/cathode and electrolyte/cathode are close to the maximum values, the overpotenial next to the electrolyte/cathode surface, i.e., $Z/L_Z = 1$, is still much higher because of higher polarization potential difference in this region. Actually, the activation loss contributes to the major portion of the overpotential. The corresponding average concentration loss is given in Fig. 8(b). It indicates that this loss is negligible compared with the activation loss under the lower current density. However, when the current density is enhanced due to a larger potential difference, the concentration loss cannot be neglected any more. For example, when the potential is 0.4 V, the maximal concentration loss is about 0.0325 V that is responsible for 9% of the total loss.

5.3. Optimization of cathode design

5.3.1. Porosity effect

Fig. 2 implies that the cathode should have the best performance with the porosity exceeding 0.3 in terms of the effective porosity. But how the porosity exactly influences the mass transfer and electrochemical behavior still needs to be further

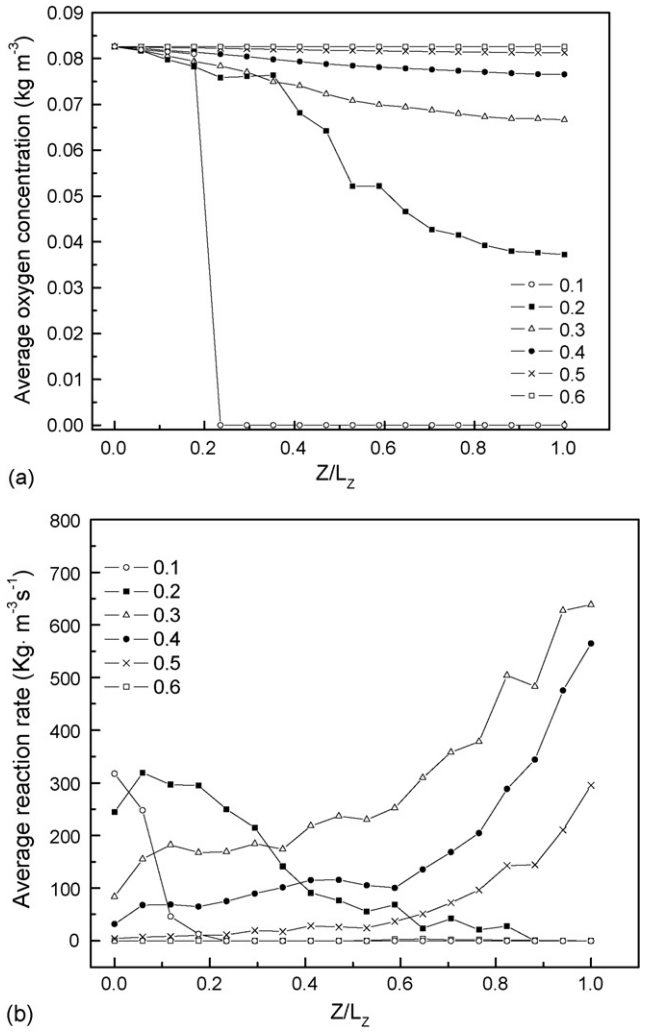

Fig. 9. Effect of porosity on performance: (a) average local oxygen concentration; (b) average reaction rate.

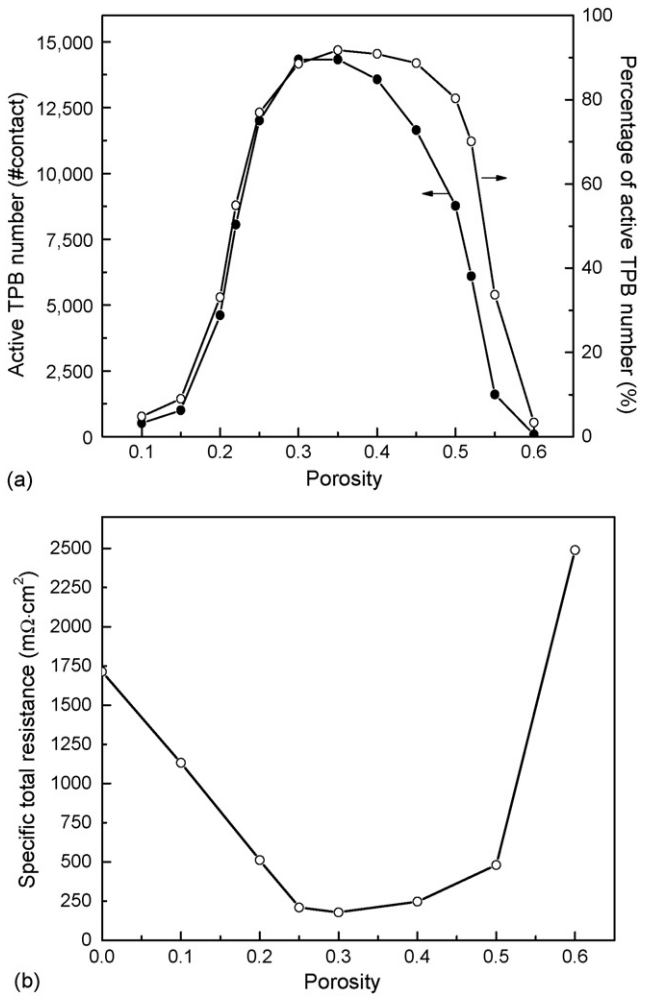

Fig. 10. Profiles of number of TPB and specific total resistance with respect to the porosity: (a) total number of active TPB; (b) specific total resistance.

investigated. The average oxygen concentration distribution and reaction rate as a function of porosity are shown in Fig. 9(a) and (b), respectively. The porosity is varied from 0.1 to 0.6 while keeping other parameters the same as that listed in Table 1. Clearly, when the porosity is at a relatively lower level, i.e., 0.1 or 0.2, the oxygen penetration depth is considerably small, only 25% of the cathode thickness for $\varepsilon = 0.1$, which will lead to a larger concentration overpotenital. The peak value of reaction rate occurs near the gas/electrode interface. This is due to the fact that an "isolated pore" dominates the whole electrode and blocks the gas supply to the TPB, and then substantially reduces the gas penetration depth. Therefore, the availability of oxygen supply and reaction sites is confined to a very narrow zone next to the gas/electrode interface. Nevertheless, when the porosity is equal to 0.3, the reaction rate begins to have a continuous tendency to increase along the thickness and also possesses the highest reaction rate. When the porosity is enhanced to 0.4 or more, the cathode performance deteriorates due to insufficient reaction sites.

Fig. 10(a) shows the statistical characters of the active TPB with respect to the porosity. It is observed that when the porosity ranges from 0.25 to 0.45, the percentage of active TPB number lies between 77% and 91%, which means the most of transport ionic or electronic particles are available to the electrochemical reaction. Therefore, in light of the above results, it can be concluded that the concentration loss can be neglected and the cathode performance reaches the best when the porosity is in the range of 0.25–0.45. In Sunde's study [18], it is assumed that all of solid particles are always available for reaction and the oxygen supply is not limited in the vicinity of a TPB. Therefore, their results are only valid for the porosity range in the middle level and also in general the resistance is underestimated in their study. The corresponding total resistance excluding the mass transfer resistance vs. porosity is plotted in Fig. 10(b). The maximum performance is achieved when $\varepsilon = 0.3$. When the porosity is equal to zero, the total resistance drastically increases by almost ten times, since there are still some active TPB's on the gas/cathode interface. On the other hand, the reaction sites completely disappear and the resistance goes to infinity when not any pore exists in the cathode. The above results have sufficiently demonstrated the porosity 0.5 is the upper limit and 0.3 is the lower limit of porosity in a composite cathode.

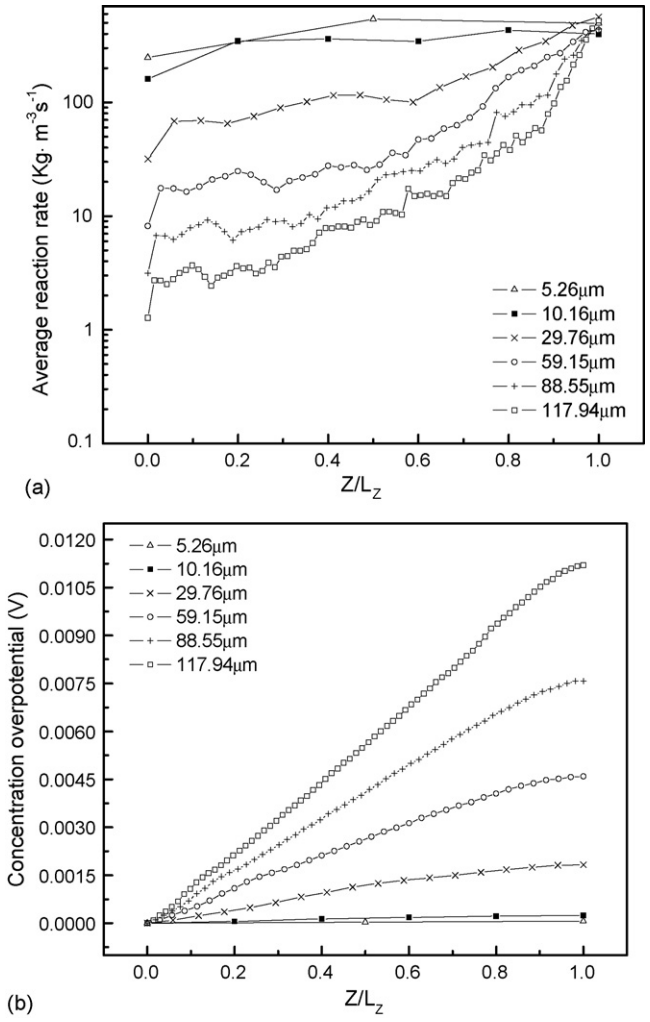

Fig. 11. Effect of thickness on reaction rate and concentration overpotential: (a) local average reaction rate; (b) local average concentration overpotential.

5.3.2. Layer thickness effect

To discover the dependence of the reaction rate and overpotentials on the cathode thickness, several cases with different thicknesses are employed. Fig. 11 gives the comparison results. When the thickness is less than 30 μm, the curve for the reaction rate is almost flat, i.e., almost all active bonds of the cathode are used; no matter how far they are from the gas/cathode interface. However, when the thickness is increased beyond 30 μm, only the zone which is close to the electrolyte/cathode is well utilized for reaction as shown in Fig. 11(a). The same tendency is also demonstrated in Costamagna et al.'s study [4]. A parameter, i.e., "effectiveness factor λ" is defined as a criterion to indicate what extent the electrode is utilized. When λ is greater than 0.3 and one of two phases has much higher resistivity than the other phase, the major part of the electrode becomes useless and the activation overpotential (or reaction) is concentrated on the electrolyte/cathode interface. Moreover, with increasing thickness, the concentration loss will become more and more significant as shown in Fig. 11(b) due to longer diffusion path and poor gas supply. Comprehensively considering the above results, suggested that the cathode thickness should be less than 89 μm here to achieve minimized concentration loss and uniform reaction rates.

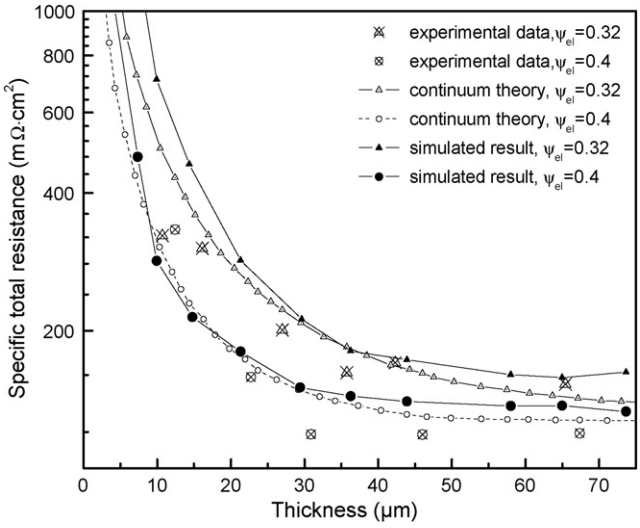

Fig. 12. Comparison among the model prediction, experimental data and continuum model.

5.3.3. Combined effect of composition, particle size and thickness

One of the important criteria indicating the electrode performance is the total specific resistance. Some experimental results have demonstrated the possibility of optimized geometrical parameters to minimize the resistance. In this section, we will consider the combined effects of composition, particle size and thickness on this resistance. The validation of the model with the experimental data and other theoretical study is presented in Fig. 12. We have incorporated literature experimental parameters and some reasonable approximated values [4,29,30] for an EDB/Pt cathode into our model, e.g., $\varepsilon = 0.4$, $T = 900\,^{\circ}\mathrm{C}$, $\gamma = 60^{\circ}$, $\varepsilon = 0.4$, $r_{el} = 0.1\,\mu\mathrm{m}$, $r_{io} = 0.1\,\mu\mathrm{m}$, $\sigma_{0,el} = 2.5 \times 10^6\,\mathrm{S\,m^{-1}}$, $\sigma_{0,io} = 20\,\mathrm{S\,m^{-1}}$. Kenjo et al. [29,30] does not give a relationship between overpotential and exchange current density such as Eq. (9), but an approximation for exchange current density, i.e., $i_0 = 400\,\mathrm{A\,m^{-2}}$ was reported by the same authors and this value has been adopted in our model. The predicted results are in good agreement with the experimental data by Kenjo et al. [29,30]. When the thickness exceeds a certain value L^*, the specific polarization levels off, keeping an almost constant trend. This can be explained by that the electronic conductor is close to a pure conductor $\sigma_{el} \gg \sigma_{io}$, the charge flows through an electronic conductor without any ohmic losses and the most of electrochemical reactions occurs in a narrow region next to the electrolyte/cathode with the thickness is increased as shown in Fig. 11(a). Therefore, the electrode resistance does not increase as the ohmic losses are negligible. Compared with the results from a continuum theory, there is a significant derivation as the electrode is very thin (<10 μm). This derivation becomes more remarkable for the case of a lower electrode volume fraction $\varphi = 0.32$. The resistance calculated from our model is higher than that from Costamagna et al.'s model [4]. The continuum theory implies

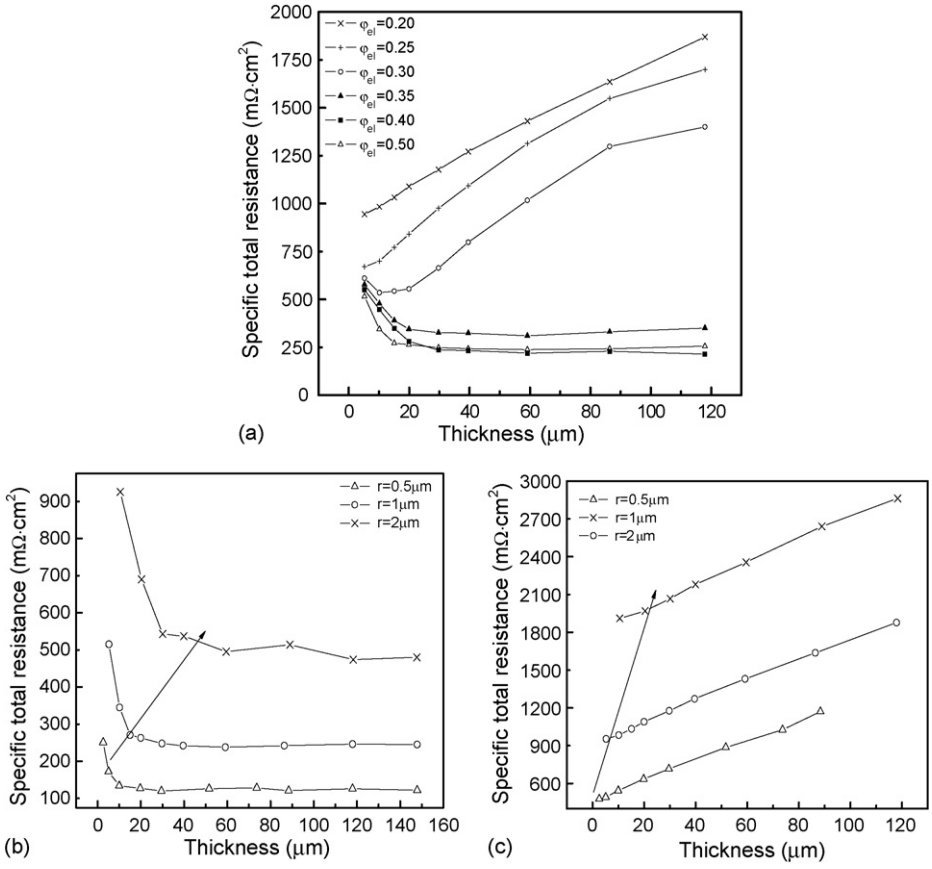

Fig. 13. Effect of electrode fraction volume and particle radius on total resistance: (a) for different φ_{el}; (b) $\varphi_{el} = 0.4$ and different radius; (c) $\varphi_{el} = 0.2$ and different radius.

an assumption that only "percolation cluster" dominates the performance and the "isolated" and "dead-end" clusters are negligible. Therefore, for a very thin electrode in which that the percolating cluster almost vanishes, this theory tends to underestimate the resistance. For a thicker electrode, the consistency between the two models is satisfactory. For the case with $\varphi_{el} = 0.32$, our model reveals a smaller value of L^*, while Costamagna et al.'s result indicates a larger L^* value and gradual decrease in resistance before $Z < 75$ μm. Simulated results sufficiently indicate that our model can well predict the experimental data.

Fig. 13 presents the combined effects of electrode volume fraction, thickness and radius of particle on the total resistance. The continuum theory and the theory of coordination number demonstrate that the percolation threshold varies from 0.294 to 0.709 as the radius ratio r_{el}/r_{io} equals to unity. Within these thresholds, reasonable performance of the cathode can be achieved. The resistance distribution within the cathode as a function of the electrode fraction is displayed in Fig. 13(a). The porosity, radius and electrode volume fraction are fixed at $\varepsilon = 0.4$, $r_{el} = r_{io} = 1$ μm and $\sigma_{el} = 0.5$, respectively. When the electrode fraction is equal to 0.35, 0.4 and 0.5, respectively, the resistance maintains a constant after a certain thickness value and the cathode thickness corresponding to the optimum performance is in the range from 17.5 to 40 μm. The maximal performance is achieved at $\varphi_{el} = 0.4$, and $Z = 29.14$ μm. However, for cases with $\varphi_{el} \leq 0.3$, the resistances become very large due to insufficient reaction sites. If considering a cathode only composed of the LSM phase with parameters: $L_Z = 29.76$ μm, $r_{el} = r_{io} = 1$ μm, $\varepsilon = 0.4$, the calculated total resistance is about 1695 mΩ cm^2. Compared this value with the data shown in Fig. 13(a), the advantage of a composite cathode is clear. From Fig. 13(b) and (c), it can be observed that with the decreasing of the radius, the optimal thickness corresponding to minimal total resistance also decreases when the electrode fraction is within the thresholds. This implies that the larger particle size, the thicker the cathode is needed to reach an optimum performance. While beyond the suggested percolation, i.e., $\varphi_{el} = 0.2$, the optimum thickness does not exist for all three cases. Therefore, the performance of a cathode can be improved by decreasing the particle size and thus enhancement in the TPB length per unit volume. However, very small LSM or YSZ particles correspondingly increase the gas diffusion path and make the pore size become smaller, so the concentration overpotential will increase, especially for a much thicker cathode.

6. Conclusions

A 3D random micro-scale model taking into account of the gas diffusion and pore structure has been developed to evaluate the mass transfer and electrochemical performance for a composite cathode in a solid oxide fuel cell. Then, detailed inves-

tigations are carried out to optimize the geometry parameters. A comparison with literature experimental data shows a good agreement.

Model results demonstrate that the concentration loss is insignificant only when the porosity is in the middle range and the cathode is thin under a lower current density. The electrochemical reaction behavior is strongly influenced by the porosity value. Only when the porosity is in the range from 0.25 to 0.45, the gas penetration depth is larger, reaction rate is relatively uniform and almost all of the TPB sites become the active TPB sites. On the one hand, the larger thickness is favorable for the performance by increasing the number of the effective reaction sites and decreasing the specific resistance. While on the other hand, the thickness should be limited to less than a certain level in order to avoid excessive concentration loss and lower utilization. Smaller particle sizes reduce activation overpotential by increasing the TPB length per unit volume of the cathode. The minimum value in total specific resistance decreases as the particle radius is decreased. But at the same time, too small particles will increase the gas diffusion resistance. In the present study, the best performance is achieved at $\varphi_{el} = 0.4$, and $Z = 29.14\ \mu m$ when $\varepsilon = 0.4$.

There is a good agreement between our predicted results with the continuum theory and experimental data. It shows that the predicted results on total specific resistance are reasonably larger than that obtained from the continuum theory for a very thin cathode. The presented model is still valid for the cathode with a lower ratio between the thickness and particle diameter compared with the continuum theory. Also, the current model removes some weaknesses in the Sunde's model [18,19], such as ignoring the diffusion resistance and specific pore structure. Therefore, this model can be applied to much more general situations.

Acknowledgements

This research was supported by the NASA Hydrogen Research for Spaceport and Space Based Applications at the University of Florida (Grant number NAG3-2930). The support by the Andrew H. Hines, Jr./Progress Energy Endowment Fund is also acknowledged.

References

[1] J. Fleig, Annu. Rev. Mater. Res. 33 (2003) 361–382.
[2] S.B. Alder, Chem. Rev. 104 (2004) 4791–4843.
[3] D.K. Kim, G.D. Kim, J.W. Moon, H.W. Lee, Li, K.T. Kim, Solid State Ionics 133 (2000) 67–77.
[4] P. Costamagna, P. Costa, V. Antonucci, Electrochem. Acta 43 (1998) 375–394.
[5] R. Zallen, The Physics of Amorphous Solids, Wiley, New York, 1983 (chapter 4).
[6] D. Bouvard, F.F. Lange, Acta Metall. Mater. 39 (1991) 3083–3090.
[7] C. Kuo, P.K. Gupta, Acta. Metall. Mater. 43 (1995) 397–403.
[8] D.S. Mclachlan, M. Blaszkiewicz, R.E. Newhanm, J. Am. Ceram. Soc. 73 (1990) 2187–2203.
[9] S. Kirkpatrick, Rev. Mod. Phys. 45 (1973) 574–588.
[10] S. Jiang, J.B. Wanger, J. Phys. Chem. Solids 56 (1995) 1113–1124.
[11] X.J. Chen, S.H. Chan, K.A. Khor, Electrochem. Acta 49 (2004) 1851–1861.
[12] D.H. Jeon, J.H. Nam, C.J. Kim, J. Electrochem. Soc. 153 (2006) A406–A417.
[13] B. Berkowitz, R.P. Ewing, Surv. Geophys. 19 (1998) 23–72.
[14] D.G. Han, G.M. Choi, Solid State Ionics 106 (1998) 71–87.
[15] J.M. Zalc, S.C. Reyes, E. Iglesia, Chem. Eng. Sci. 58 (2003) 4605–4617.
[16] F.J. Keil, Catal. Today 53 (1999) 245–258.
[17] L. Zhang, N.A. Seaton, Chem. Eng. Sci. 49 (1994) 41–50.
[18] S. Sunde, J. Electrochem. Soc. 143 (1996) 1123–1132.
[19] S. Sunde, J. Electrochem. Soc. 143 (1996) 1930–1938.
[20] A. Loselevich, A.A. Kornyshev, W. Lehnert, J. Electrochem. Soc. 144 (1997) 3010–3019.
[21] G.N. Constatinides, A.C. Payatakes, Chem. Eng. Commun. 81 (1989) 55–81.
[22] C. Ciobanu, Y. Liu, Y. Wang, B.R. Patton, J. Electroceram. 3 (1999) 17–23.
[23] P.H. Winterfeld, L.E. Scriven, H.T. Davis, J. Phys. C: Solid State Phys. 14 (1981) 2361–2376.
[24] M. Sahimi, T.T. Tsotsis, J. Catal. 96 (1985) 552–562.
[25] A.F. Mills, Mass Transfer, Prentice Hall, 2001.
[26] J. Abel, A.A. Kornyshev, W. Lehnert, J. Electrochem. Soc. 144 (1997) 4253–4259.
[27] Y. Ji, K. Yuan, J.N. Chung, Y.C. Chen, J. Power Sources 161 (2006) 380–391.
[28] J. Hoshen, R. Kopelman, Phys. Rev. B 14 (1976) 3438–3445.
[29] T. Kenjo, S. Osawa, K. Fujikawa, J. Electrochem. Soc. 138 (1991) 349–356.
[30] T. Kenjo, M. Nishiya, Solid State Ionics 57 (1992) 295–302.